Radiomics-Based Distinction of s-HCC and Precancerous Lesion Based on Precontrast MRI

JiaWen Luo
Second Affiliated Hospital of Dalian Medical University
Kun Guo
Second Affiliated Hospital of Dalian Medical University
XiaoNing Gao (748117050@qq.com)
Second Affiliated Hospital of Dalian Medical University
Hao Liu
Yizhun Medical AI Co., Ltd, Beijing, China
Yue Xiang
Second Affiliated Hospital of Dalian Medical University
Jia Ding
Yizhun Medical AI Co., Ltd, Beijing, China

Research Article

Keywords: Radiomics, s-HCC, MRI

Posted Date: May 27th, 2021

DOI: https://doi.org/10.21203/rs.3.rs-545379/v1

Abstract

Background: To assess the feasibility of radiomics based on precontrast MRI for the distinguish of s-HCC and pre-HCC.

Method: We retrospectively analyzed 146 nodules from 78 patients, with pathological confirmed. Each nodule was segment on precontrast MRI sequence(TIWI and fat-suppression T2WI), retrospectively. 1223radiomics features were extracted and the optimal 10 features were selected by LASSO to establish the logistic regression radiomics model.

Result: The AUC, sensitivity and specificity of the training group and test group were 0.757 (95% CI 0.638 -0.853), 83.02% , 66.67% and 0.789 (95% CI 0.643-0.895), 88.89% and 80.00%, respectively. The AUC, sensitivity and specificity of the training group and test group were 0.903 (95% CI 0.807-0.962), 86.79% , 86.67% and 0.778 (95% CI 0.632-0.887), 75.00%, 80.00%, respectively. Delong test has proved that, the diagnositic performances of radiomics model based on T2WI were higher than that of radiomics model based on T1WI (p = 0.0379).

Conclusion: Radiomics model can classify s-HCC and pre-HCC based on precontrast MRI. And may serve as an adjunct tool for accurate diagnosis of s-HCC.

Background

Hepatocellular carcinoma (HCC) is the fifth most common tumor and the second most fatal cancer in the world [1]. Most HCC develops through a multistep process, called hepatocarcinogensis, in which regenerative nodule, low-grade dysplastic nodule and high-grade dysplastic nodule (referred as pre-HCC) evolves into early-HCC and pro-HCC gradually [2,3]. The prognosis of HCC depends largely on the stage at which the tumor is detected [4]. Patients may benefit from life-prolonging, potentially curative treatments in the early [5]. Some clinical studies have shown that clinical surgical intervention for s-HCC (≤ 2cm) can reduce the recurrence rate and improve the cure rate of patients [6-8]. Therefore, early detection of s-HCC is of great significance for patients at high risk of HCC. All current guidelines recommend surveillance for patients at high risk. In general, CT and MRI with contrast agent are common used. A diagnosis of HCC can be made noninvasively until typical HCC features are present. At present, Gd-EOB-DTPA MRI and DWI are commonly used to improve the detection rate and diagnostic accuracy of s-HCC. Renzulli et al. demonstrated that a new diagnostic algorithm combined with Gd-EOB-DTPA MRI and DWI could evaluated all the lesions in a cirrhotic liver, including early HCC and HGDN [9]. However, diagnosis may be problematic in patients who cannot undergo enhancement inspection because of contraindications. Moreover, multiple enhancement examinations will increase the burden of patients. We urgently need a more convenient method.

Radiomics, as a quantitative noninvasive analysis method, has shown great application value in diagnosis, evaluation of curative effect and prognosis. Gato et al. suggested that radiomic can classify focal liver lesions based on non-enhanced T2-weighted images [10]. Wu et al. showed that radiomics can

be used to distinguish between HCC and hepatic haemangioma on precontrast images [11]. Li et al. reported texture features of SPAIR T2WI-MRI can classify the three types of single liver lesions (HH, HM and HCC) [12]. This study aims to assess the feasibility of radiomics based on precontrast MRI for differentiation of s-HCC and pre-HCC.

Material And Methods

Patient

This is a retrospective study. Between September 2017 and February 2020, 82 consecutive patients were included in this study and evaluated by precontrast MRI. The exclusion criteria were as follows: patient underwent any preoperative intervention treatment; the lesion was not clearly shown on precontrast MRI; nodule larger than 2cm; patient did not undergo resection or liver transplantation; the gross specimen did not correspond to the location and size of the nodules shown in the imaging; pathological diagnosis of the nodule was not s-HCC or pre-HCC.

MRI acquisition

All enrolled patients were examined with 3.0T MRI (Verio; Siemens, Erlangen, Germany), with 8-channel body phased array coil and TSE sequence acquisition collection under respiratory trigger. Abdominal pressure band was applied to the lower abdomen of the patient to reduce artifacts caused by abdominal respiratory movements. The scanning sequence of MRI included: axial TIWI and axial fat-suppression T2WI. The parameters of each MRI sequence are shown in Table 1.

Table 1. MRI conventional sequence parameter

TR（ms）	TE(ms)	Matrix	thickness (mm)	slice gap (mm)	NEX
Axial T1WI	200	2.2	256´160	5	0	1
Axial fs T2WI	infinite	8.5	288´256	5	1	2

Pathological examination

Refer to the MRI image, the liver resected or transplantation specimens were cut at an interval of nearly 1cm. The dissected liver specimens were corresponding to the abnormal signal nodules shown in the images. Pathological specimens were sectioned, dehydrated and paraffin-embedded, stained with hematoxylin-eosin (HE), and then subjected to histological and immunohistochemical examination. The pathological diagnosis of nodule was evaluated according to the International Consensus Group for Hepatocellular Neoplasia criteria. Two pathologists with more than 10 years of experience in HCC pathology reviewed all the specimen slices independently, without knowing the patients' clinical data.

Model establishment and comparison

Establishment of radiomics model

1. *Segmentation*

The volumes of interests (VOIs) were delineated around the liver nodules' outline for 3D volume area as indicated in TIWI and fat-suppression T2WI by two independent radiologists with more than 5 years of experience in abdominal diagnosis. Segmentation was checked by a radiologist with over 10 years of experience in abdominal diagnosis. All three radiologists were blinded to pathological results, but were aware of the purpose and method of the study.

2. *Extraction and selection*

The first is the normalization of image quantitative data. We normalized the pixels to 1:1:1, and linearly normalized the grayscale values from 0 to 4096. The radiomics features are extracted from the image by mathematical algorithm software, mainly include first-order features, 2D and 3D shape features, texture features (including gray-level co-occurrence matrix (GLCM) features, gray-level run-length matrix (GLRLM) features, gray-level size zone matrix (GLSZM) features , gray-level dependence matrix (GLDM) features, and neighbourhood gray-tone difference matrix (NGTDM) features)[12]. A total of 1223 radiomics features were extracted from each sequence. To avoid overfitting, the least absolute shrinkage and selection operator (LASSO) algorithms was applied for dimensionality reduction. Finally, the optimal 10 features were selected from each sequence .

3. *Establishment of radiomics model*

Logistic Regression (LR) was applied to establish two radiomics models using the optimal 10 radiomics features selected from T1WI, T2WI, respectively[11]. Radiomics models were evaluated using the area under the receiver operating characteristic curve (AUC) .

Comparison

Delong test was used to compare the AUCs of T1WI, T2WI radiomics models.

Statistic analysis

Statistical analysis were carried out using Medcale statistical software (http://www.medcalc.org). Radiomics feature extraction, dimension reduction and model establishment were accomplish by the Medical Standard - Darwin Intelligent Scientific Research Platform (Beijing, Yizhun Medical AI Co., Ltd).

Results

1. **Characteristics of patients and nodules**

A total of 78 patients with 114 nodules were included in the study except 4 patients who had severe ascites. 70 patients had chronic hepatitis B cirrhosis, 3 patients had chronic hepatitis C cirrhosis, 3

patients had autoimmune cirrhosis, and 2 patients had alcoholic cirrhosis. There were 89 s-HCCs and 25 pre-HCCs, including 3 DNs and 22 RNs.

2. **Radiomics models**

The flow chart for the establishment of radiomics model is shown in Fig. 1.

The optimal radiomics features and radiomics scores obtained based on T1WI are shown in Formula 1. The AUC, sensitivity and specificity of the training group were 0.757 (95% CI 0.638 -0.853), 83.02% and 66.67%, respectively. The AUC, sensitivity and specificity of the test group were 0.789 (95% CI 0.643-0.895), 88.89% and 80.00%,respectively. The ROCs of the models are shown in Fig. 2.

RadScore = -1.533*T1WI_wavelet-LHL_glcm_InverseVariance+

1.083*T1WI_wavelet-HLL_firstorder_Mean+

0.851*T1WI_wavelet-HLL_firstorder_Median+

0.558*T1WI_wavelet-HLL_firstorder_Minimum-

0.525*T1WI_wavelet-LHL_firstorder_InterquartileRange-

0.477*T1WI_wavelet-HLH_glcm_Autocorrelation-

0.460*T1WI_wavelet-HLH_gldm_LargeDependenceHighGrayLevelEmphasis-

0.460*T1WI_wavelet-HLH_gldm_HighGrayLevelEmphasis-

0.187*T1WI_wavelet-HHL_firstorder_InterquartileRange-

0.049*T1WI_wavelet-HHL_firstorder_90Percentile-0.688 **Formula (1)**

The optimal radiomics features and the radiomics score obtained based on T2WI are shown in Formula 2. The AUC, sensitivity and specificity of the training group were 0.903 (95% CI 0.807-0.962), 86.79% and 86.67%, respectively. The AUC, sensitivity and specificity of the test group were 0.778 (95% CI 0.632-0.887), 75.00%, and 80.00%, respectively. The ROCs of the models are shown in Fig. 3.

RadScore = -1.584*T2WI_wavelet-HLL_firstorder_Mean-

1.512*T2WI_wavelet-LHL_firstorder_Median-

1.487*T2WI_wavelet-HLL_ngtdm_Contrast-

1.318*T2WI_wavelet-LHL_firstorder_Mean-

0.959*T2WI_square_gldm_DependenceNonUniformityNormalized-

0.618*T2WI_square_gldm_LargeDependenceLowGrayLevelEmphasis-

0.425*T2WI_wavelet-HLL_firstorder_Median-

0.414*T2WI_square_glcm_MaximumProbability-

0.279*T2WI_square_glcm_JointEnergy-

0.156*T2WI_square_glszm_SizeZoneNonUniformityNormalized+3.391 **Formula** (2)

3. **Comparison of diagnostic performance**

Delong test has proved that, the diagnositic performances of radiomics model based on T2WI were higher than that of radiomics model based on T1WI (p = 0.0379).

Discussion

In this study, we used radiomics, a noninvasive and quantitative method, to distinguish s-HCCs and pre-HCCs using precontrast MR-based radiomics features. The aim of our study was to assess the feasibility of radiomics to diagnose s-HCCs. Our result revealed that T2WI-based radiomics model showed better performance in identifying s-HCC.

We would like to analysis the valuable 10 features extracted from T2WI, including first-order, second-order and higher-order (GLSZM (gray level size zone), NGTDM (neighbouring gray tone difference matrix) and GLDM (dependence non-uniformity normalized)) [13]. First-order features describe the spatial distribution of multiple voxel intensities regardless of the three-dimensional. First-order_mean and _median mean the average and median gray level intensity within the ROI, respectively [13]. Second-order and higher-order are generally named as “texture” features, which are described a density of each pixel via histogram and the spatial locations. There are some meaningful features. GLSZM_size zone non-uniformity measures the variablility of size zone volumes throughout the image. NGTDM_contrast is a measure of the spatial intensity change, and it also dependent on the overall gray level dynamic range. GLDM_dependence non-uniformity and _large dependence low gray level emphasis features all indicate the homogeneity of ROI [13].

These features maybe strongly related to the different pathological features between s-HCC and pre-HCC. We would discuss below. The key pathologic alterations of pre-HCCs are consistent with the change in the multistep hepatocarcinogenesis process, in which a series of cytological and architectural atypia will occur. First, that large and small cell changes are observed in terms of cellular and nuclear sizes of hepatocytes, staining of the cytoplasm, and degree of nuclear pleomorphism [14, 15]. Second, pathological studies have revealed that fat modification, iron or copper accumulation are encountered [16, 17]. Thirdly, architectural atypia mainly includes decreased portal tracts, progressive sinusoidal capillarization, recruitment of unpaired arterioles, and alteration of the venous drainage system [18–21].

These different pathological features between s-HCC and pre-HCC can be reflected in MRI. However, above-mentioned pathological features are difficult to distinguish with the naked eyes, whereas they could be presented as quantitative radiomics features. Cause of the repeatability and non-fatigue characteristics of the radiomics, it has potential clinical application value. In this study, we delineated around each lesion outline for 3D volume area to obtain whole radiomics features. To make precise classification, we also certified all lesions by postoperative pathology. Thus, it is a reliable and noninvasive method for differential diagnosis between s-HCC and pre-HCC.

And why T2WI features showed better performance? Shinmura et al. found that there was a significant association between the intranodular portal venous and arterial blood supplies and the T2-weighted MR imaging signal intensity in various types of hepatocellular nodules associated with liver cirrhosis [22]. Namely, the signal intensity on T2-weighted MR images increased as the intranodular portal venous blood supply decreased and arterial supply increased [22]. The conclusions may also be applicable to distinguish s-HCC and pre-HCC. Furthermore, because of different iron, fat, and copper accumulations in cell during hepatocarcinogenesis, T2WI shows different signal of s-HCC and pre-HCC. Generally speaking, T2WI showed dominant discrepancy between lesions and peripheral liver tissue. And, the random errors such as segmentation and ROI drawing may also cause differences between T1WI and T2WI performance [23].

Mokrane et al validated Delta V-A_DWT_LL_Variance-2D, a single radiomics feature of CT, which quantifying changes between arterial and portal venous phases can diagnose HCC in cirrhotic patients with indeterminate liver nodules [24]. Our radiomic features were extracted from precontrast MRI, ignoring the contraindication of enhanced scanning.

There are several limitations to this study. Firstly, the sample size is small. A large number date from multi-center can validate and improve the generalisability of our finding. Secondly, other MRI sequences, such as in-, out-phase and DWI, would be enrolled in further studies to verify its utility. Thirdly, clinical characteristic may be helpful in distinguishing s-HCCs from pre-HCCs and should be further studied.

This study suggested that radiomics features may related to the microscopic features of s-HCCs and pre-HCCs. can capture the microscopic features of s-HCC and pre-HCC and gives a noninvasive efficient method to distinguish s-HCCs and pre-HCCs. Future studies should be validated and improved for higher reliability.

Abbreviations

AUC: Area under receiver operating characteristic curve; GLCM: Gray-level co-occurrence matrix; GLDM: Gray-level dependence matrix; HCC: Hepatocellular carcinoma; HGDN: High grade dysplastic nodule; LGDN: Low grade dysplastic nodule; LR: Logistic regression; MRI: Magnetic resonance imaging; NGTDM: Neighbourhood gray-tone difference matrix; Rad score: Radiomics score; RN: Regenerative nodule; ROC: Receiver operating characteristic curve; s-HCC: small-Hepatocellular carcinoma; TSE: Turbo spin-echo; VOI: volume of interest

Declarations

Acknowledgements

The authors wish to thank Hao Liu, Ph.D. and Jia Ding, Ph.D. for their technical support in the instructions of the radiomics analysis.

Funding

There is no funding.

Availability of data and materials

The datasets generated and/or analysed during the current study are not publicly available due to patient privacy protection, but are available from the corresponding author on reasonable request.

Authors' contribution

XNG and JWL conceived the research, executed the experiments, and wrote the manuscript. XNG, KG and YX did some work in performing the experiments. HL and JD analyzed the result. All authors read and approved the final manuscript for publication.

Ethics approval and consent to participate

This study was approved by the institutional review board at the corresponding author's institution(The Second Affiliated Hospital of Dalian Medical University), and follow the principles of the 1964 Declaration of Helsinki and subsequent amendments. Informed consent was obtained from all patients. The consent obtained from study participants was verbal because this retrospective study has been approved by the ethics committee at the corresponding author's institution.

Consent for publication

Consent for publication of individual persons' images was obtained from these persons.

Competing interests

The authors declare that they have no competing interests.

Publisher's note

References

1. Heimbach JK, Kulik LM, Finn RS, Sirlin CB, Abecassis MM, Roberts LR, et al. AASLD guidelines for the treatment of hepatocellular carcinoma. Hepatology 2018;67:358–380.
2. Coleman WB. Mechanisms of human hepatocarcinogenesis. Curr Mol Med. 2003;3:573–88.

3. Efremidis SC, Hytiroglou P. The multistep process of hepatocarcinogenesis in cirrhosis with imaging correlation. Eur Radiol. 2002;12:753–64.
4. McGlynn KA, London WT. Epidemiology and natural history of hepatocellular carcinoma. Best Pract Res Clin Gastroenterol 2005;19 (1): 3–23.
5. Choi J Y, Lee J M, Sirlin C B. CT and MR Imaging Diagnosis and Staging of Hepatocellular Carcinoma: Part I. Development, Growth, and Spread: Key Pathologic and Imaging Aspects[J]. Radiology, 2014, 272(3):635–654.
6. Takayama T, Makuuchi M, Hirohashi S, et al. Early hepatocellular carcinoma as an entity with a high rate of surgical cure. Hepatology 1998; 28:1241–46.
7. Midorikawa Y, Yamamoto S, Tsuji S, et al. Allelic imbalances and homozygous deletion on 8p23.2 for stepwise progression of hepatocarcinogenesis. Hepatology 2009;49:513–22.
8. Yamamoto M, Takasaki K, Otsubo T, et al. Favorable surgical outcomes in patients with early hepatocellular carcinoma. Ann Surg 2004; 239:395–9.
9. Renzulli M, Biselli M, Brocchi S, et al. New hallmark of hepatocellular carcinoma, early hepatocellular carcinoma and high-grade dysplastic nodules on Gd-EOB-DTPA MRI in patients with cirrhosis: A new diagnostic algorithm. Gut, 2018, 67(9): 1674–1682.
10. Gatos I, Tsantis S, Karamesini M, et al. Focal liver lesions segmentation and classification in nonenhanced T2-weighted MRI[J]. Medical Physics, 2017, 44.
11. Wu J, Liu A, Cui J, et al. Radiomics-based classification of hepatocellular carcinoma and hepatic haemangioma on precontrast magnetic resonance images[J]. BMC Medical Imaging, 2019, 19(1).
12. Li Z, Yu M, Wei H, et al. Texture-based classification of different single liver lesion based on SPAIR T2W MRI images[J]. BMC Medical Imaging, 2017, 17(1):42.
13. Zwanenburg A, Leger S, M Vallières, et al. Image biomarker standardisation initiative[J]. Radiotherapy & Oncology, 2016.
14. Libbrecht L, Desmet V, Van D B, et al. The immunohistochemical phenotype of dysplastic foci in human liver: correlation with putative progenitor cells[J]. Journal of Hepatology, 2000, 33(1):76–84.
15. Anthony P P, Vogel C L, Barker L F. Liver cell dysplasia: a premalignant condition.[J]. Journal of Clinical Pathology, 1973, 26(3):217–223.
16. Kutami R, Nakashima Y, Nakashima O, et al. Pathomorphologic study on the mechanism of fatty change in small hepatocellular carcinoma of humans[J]. Journal of Hepatology, 2000, 33(2):282–289.
17. Zhang J, Krinsky G A. Iron-containing nodules of cirrhosis.[J]. Nmr in Biomedicine, 2004, 17(7):459–64.
18. Palmer W C, Patel T. Are common factors involved in the pathogenesis of primary liver cancers? A meta-analysis of risk factors for intrahepatic cholangiocarcinoma[J]. JOURNAL OF HEPATOLOGY, 2012.

19. Coleman W B. Coleman, WB. Mechanisms of human hepatocarcinogenesis. Curr Mol Med 3: 573–588[J]. Current Molecular Medicine, 2003, 3(6):573–588.
20. Ueda K, Matsui O, Kawamori Y, et al. Hypervascular hepatocellular carcinoma: evaluation of hemodynamics with dynamic CT during hepatic arteriography.[J]. Radiology, 1998, 206(1):161–6.
21. Kitao A, Zen Y, Matsui O, et al. Hepatocarcinogenesis: multistep changes of drainage vessels at CT during arterial portography and hepatic arteriography–radiologic-pathologic correlation.[J]. Radiology, 2009, 252(2):605–614.
22. Shinmura R, Matsui O, Kobayashi S, et al. Cirrhotic nodules: association between MR imaging signal intensity and intranodular blood supply.[J]. Radiology, 2005, 237(2):512.
23. Wu J, Liu A, Cui J, et al. Radiomics-based classification of hepatocellular carcinoma and hepatic haemangioma on precontrast magnetic resonance images[J]. BMC Medical Imaging, 2019, 19(1).
24. Radiomics machine-learning signature for diagnosis of hepatocellular carcinoma in cirrhotic patients with indeterminate liver nodules[J]. European Radiology, 2020, 30(1):558–570.

Figures

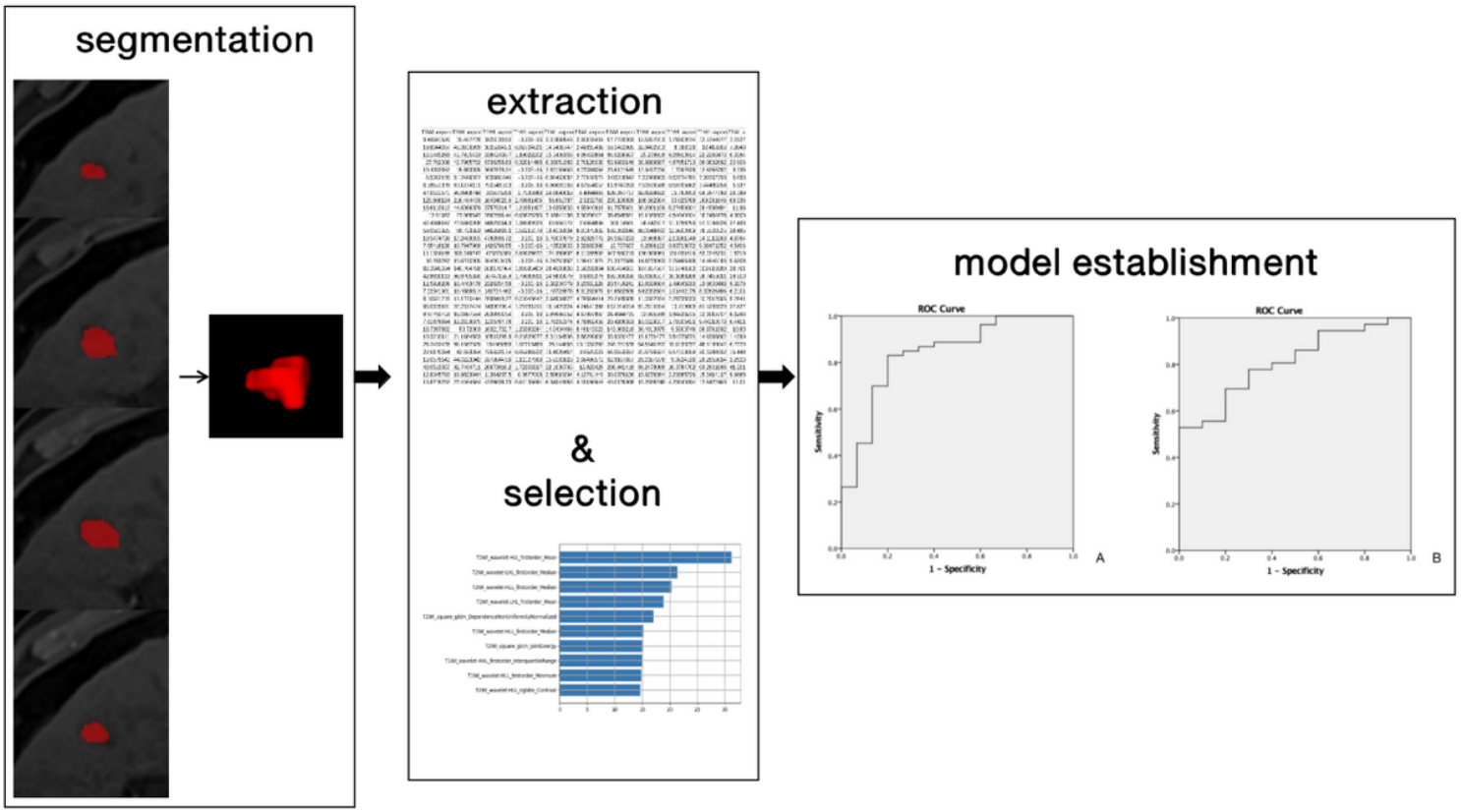

Figure 1

Flow chart of radiomics model establishment

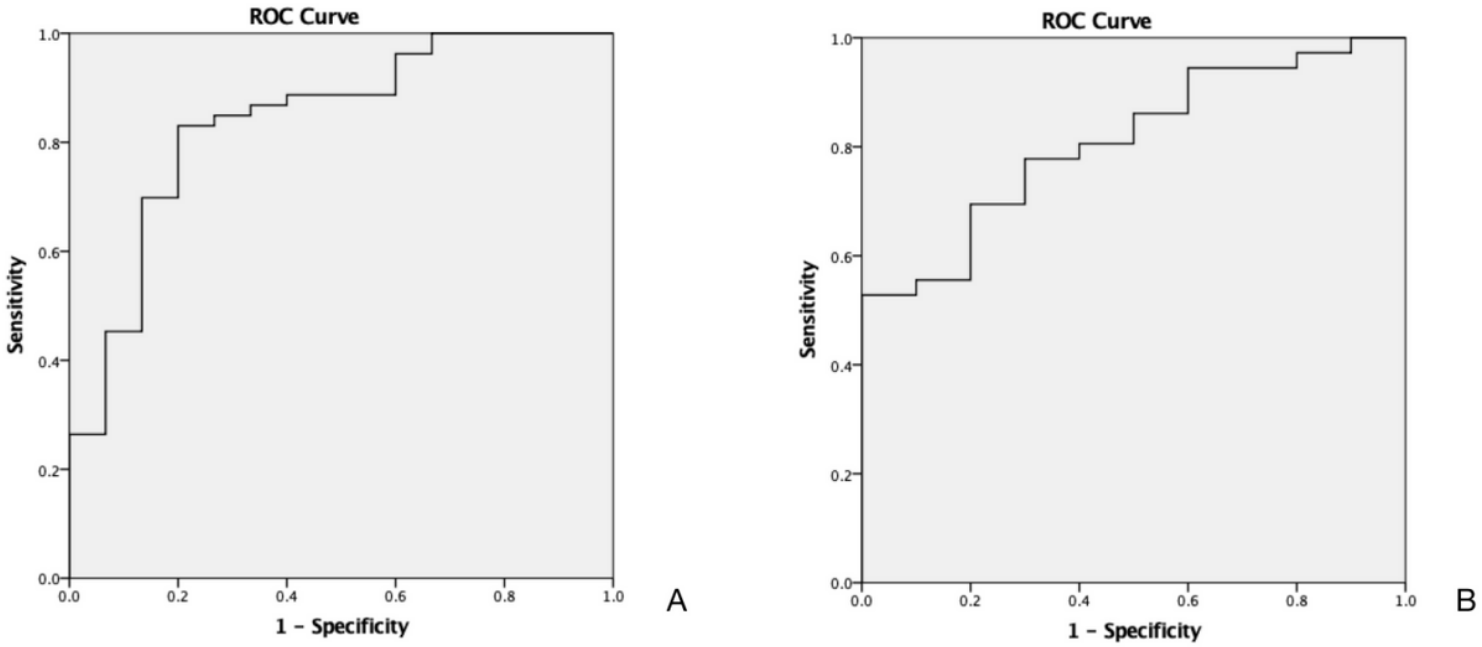

Figure 2

ROCs of radiomics model based on T1WI (A: ROC of training group; B: ROC of test group)

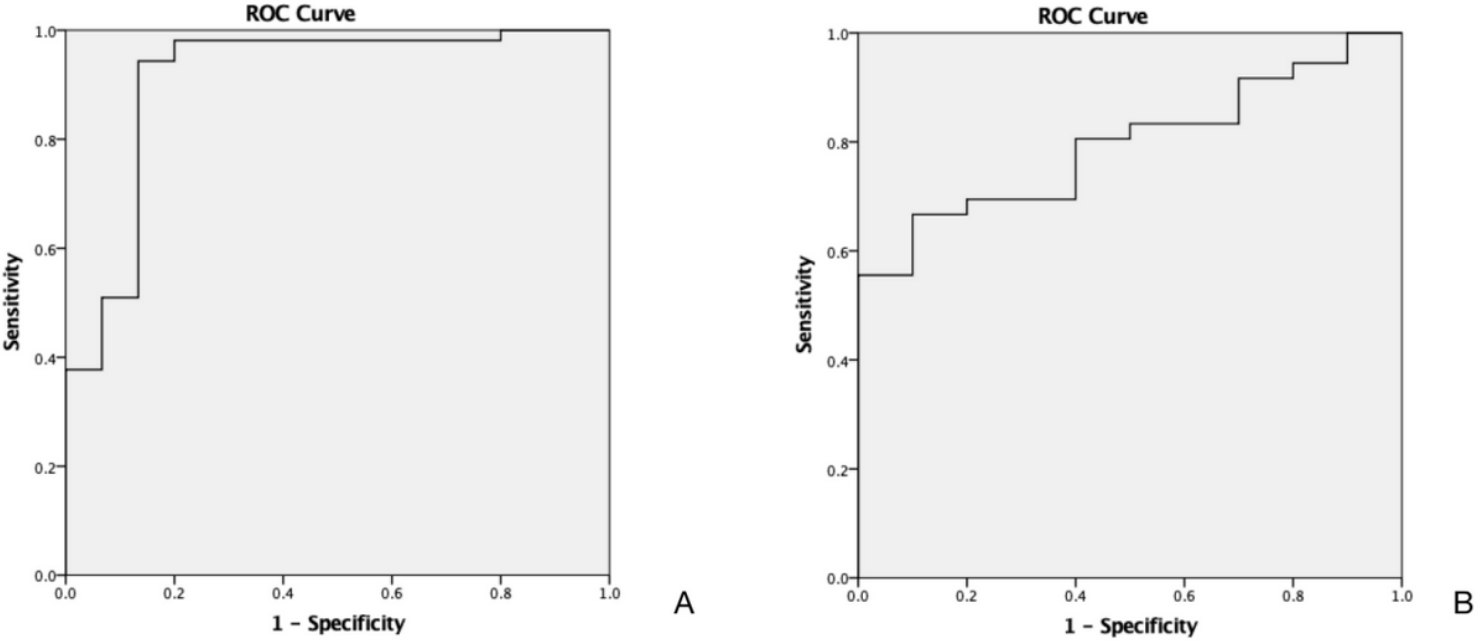

Figure 3

ROCs of radiomics model based on T2WI (A: ROC of training group; B: ROC of test group)